Eur Biophys J (1992) 21, 281–298

European Biophysics Journal

The roles of serine and threonine sidechains in ion channels: a modelling study

Mark S. P. Sansom

Laboratory of Molecular Biophysics, The Rex Richards Building, University of Oxford, South Parks Road, Oxford, OX1 3QU, UK

Received January 27, 1992/Accepted in revised form July 6, 1992

Abstract. The ion channel of the nicotinic acetylcholine receptor (nAChR) is believed to be lined by transmembrane M2 helices. A "4-8-12" sequence motif, comprising serine (S) or threonine (T) residues at positions 4, 8 and 12 of M2, is conserved between different members, anion and cation selective, of the nAChR superfamily. Parallel bundles of 4-8-12 motif-containing helices are considered as simplified models of ion channels. The relationship between S and T sidechain conformations and channel-ion interactions is explored via evaluation of interaction energies of K^+ and of Cl^- ions with channel models. Energy calculations are used to determine optimal χ_2 ($C\alpha$-$C\beta$-$O\gamma$-$H\gamma$) values in the presence of K^+ or Cl^- ions. 4-8-12 motif-containing bundles may form favourable interactions with either cations or anions, dependent upon the χ_2 values adopted. Parallel-helix and tilted-helix bundles are considered, as are heteromeric models designed to mimic the *Torpedo* nAChR. The main conclusion of the study is that conformational flexibility at χ_2 enables both S and T residues to form favourable interactions with anions or cations. Consequently, there is apparently no difference between S and T residues in their interactions with permeant ions, which suggests that the presence of T *vs.* S residues within the 4-8-12 motif is not a major mechanism whereby anion/cation selectivity may be generated. The implications of these studies with respect to more elaborate models of nAChR and related receptors are considered.

Key words: Ion channel – Nicotinic receptor – α-helix bundle – Molecular modelling

Abbreviations: nAChR, GluR, NMDA-R, $5HT_3$-R, $GABA_A$R, GlyR – nicotinic acetylcholine, glutamate, NMDA, $5HT_3$, $GABA_A$ and glycine receptors, respectively; PhTx – philanthotoxin; M2 – second membrane-spanning helix of receptor-channel subunits.

Introduction

Receptor-gated ion channels form the basis of fast synaptic neurotransmission. They are multi-subunit, integral membrane proteins which permit selected ions to move rapidly (ca. 5×10^7 s^{-1}) down electrochemical gradients across membranes. Their molecular properties are the subject of intense scrutiny, following expansion of the sequence database for this superfamily of proteins. In particular, the nicotinic acetylcholine receptor (nAChR) is the focus of investigations employing a range of biochemical and biophysical techniques (Stroud et al. 1990; Galzi et al. 1991).

Sequence comparisons between different members of the receptor-channel superfamily suggest that four putative membrane spanning regions (M1 to M4) are conserved (Betz 1990; Unwin 1989). On the basis of low resolution structural studies (Toyoshima and Unwin 1988, 1990; Mitra et al. 1989) and of chemical labelling experiments (Giraudat et al. 1987; Hucho et al. 1986) it is proposed that five M2 helices form a bundle of approximately parallel helices surrounding a central ion channel. This is supported by site-directed mutagenesis studies (Imoto et al. 1988; Leonard et al. 1988; Charnet et al. 1990; Revah et al. 1991) which correlated changes in amino acid sequence at and around the M2 region with changes conductance and selectivity. Recent sequencing studies on glutamate receptors (GluR; Hollman et al. 1989; Keinanen et al. 1990), on NMDA receptors (NMDA-R; Moriyoshi et al. 1991) and $5HT_3$ receptors ($5HT_3$-R; Maricq et al. 1991) demonstrate that the M2 region is conserved in distantly related members of the nAChR superfamily.

M2 helices are amphipathic. The hydrophilic faces, which are believed to line the channel, contain several serine (S) and/or threonine (T) sidechains (Unwin 1989; Betz 1990). Mutagenesis studies (Leonard et al. 1988; Charnet et al. 1990; Villarroel et al. 1991; Imoto et al. 1991) demonstrate that these sidechains interact with permeant ions and with channel-blocking drugs. Interestingly, serine and threonine sidechains are present in *both*

cation selective (nAChR, Glu-R, NMDA-R, $5HT_3$-R) and anion selective ($GABA_A$-R, Gly-R) channels. Anion selective channels seem to contain a higher proportion of T residues, a feature which has been suggested to be of functional importance (e.g. Stroud et al. 1990).

In a study of the conformation of S and T sidechains in helices, Gray and Matthews (1984) discussed how such hydrophilic sidechains might be buried in a hydrophobic milieu. They concluded that S and T residues, when present in an α-helix, have a propensity for forming hydrogen bonds between the hydroxyl hydrogen atom, Hγ:n, of the sidechains and a carbonyl oxygen atom, O:(n−3) or O:(n−4), of the mainchain. The current study is an attempt to incorporate such stereochemical information within a simplified model of M2 helix bundles in an effort to understand how M2 helices containing S and/or T residues may interact favourably with anions and/or cations. As in an earlier paper (Sansom 1992) emphasis is placed upon obtaining a structural model of a given sequence *motif*, in this case the S/T-containing region of M2 helices. This investigation differs from attempts to model nAChR M2 helix bundles (Furois-Corbin and Pullman, 1989a, b, 1991; Eisenman and Alvarez 1991; Stroud et al. 1990) in that an isolated motif is investigated rather than complete M2 helices (plus adjacent residues). The modelling strategy employed is similar to that used in an earlier study of channel-forming peptides (Sansom et al. 1991).

Methods

General computational methods

The following section provides a brief account of the computational methodology employed in this study. A more detailed account is provided in an earlier publication (Sansom et al. 1991). Modelling was carried out using QUANTA 3.2 (Polygen, Waltham, MA), run on a Silicon Graphics (Mountain View, CA) Personal Iris workstation. Energy minimization and empirical energy function calculations were performed using the molecular mechanics program CHARMm (V21.3; Brooks et al. 1983). Diagrams of molecular structures were drawn using MolScript (Kraulis, 1991). All auxiliary programs were written in Fortran 77.

Helix bundle models

Helix bundle generation was carried out using the program *bndlq* (Sansom et al. 1991). The first stage of this requires definition of the helix axis of the monomer. This is calculated from the midpoint of selected Cα atoms. For example, for a 23 residue α helix, the helix axis may be defined by a vector from the helix centre, given by the midpoint of Cα:1−23, to the end of the helix, given by the midpoint of Cα:20−23. The helix is aligned such that its axis is coincident with the z-axis of the coordinate system. It is rotated about z by an angle θ such that the centre of the hydrophilic face of the helix is directed along the x-axis. Thus oriented, the helix may then used to generate a parallel-helix bundle, with N monomers and with an interaxial separation of R between the centres of the constituent helices. There also exists the option to tilt the helix by rotation through an angle Ω about y axis prior to bundle generation, resulting in a (truncated) conical helix bundle (see below). Thus, the bundle is made up of helices A, B, ... with helix A positioned such that its centre lies on the x-axis, its axis is parallel to (or makes an angle Ω with) z, and its hydrophilic face points along x. The axis of the pore running down the centre of the bundle is coincident with the z-axis.

Ion-channel interactions

The aim of these calculations is to probe for possible ion-liganding sites within the pore defined by a helix bundle. They are not intended to calculate true permeation profiles for ions moving through the pore, as the models used to not include water and so fail to take into account solvation/desolvation energies of the ion. However, the results are of value in that they permit one to focus on possible ion-protein interaction within the bilayer region.

In these calculations, the channel model is treated as a rigid body (i.e. "frozen" coordinates). Polar hydrogen atoms are explicitly included, whereas non-polar hydrogens are included via an extended atom representation. An ion probe is placed at points along the z-axis. The empirical energy of interaction between ion and channel (E_T) is evaluated as the sum of a van der Waals (E_V) and an electrostatic (E_E) term:

$$E_T = E_V + E_E.$$

The van der Waals energy is given by a Lennard-Jones 6−12 potential function:

$$E_V = \sum_{i,j} \left(\frac{A_{ij}}{r_{ij}^{12}} - \frac{B_{ij}}{r_{ij}^{6}} \right) \cdot sw(r_{ij}),$$

where sw is a switching function (Brooks et al. 1983), with a cutoff distance of 20 Å. The electrostatic energy is given by:

$$E_E = \sum_{i,j} \left(\frac{q_i q_j}{4 \pi \varepsilon_{ij}} \right) \cdot sh(r_{ij}),$$

where sh is a shift function (Brooks et al. 1983), with a cutoff distance of 20 Å. Note that the electrostatic energy is calculated using a distance dependent dielectric, i.e. $\varepsilon = \varepsilon_0 r$ (Brooks et al. 1983, 1988; Rogers 1986) in order to mimic the effect of solvent-screening on ion-channel interactions at larger distances. The van der Waals parameters (A_{ij} and B_{ij}) and partial charges (q_i) of the constituent atoms were taken from the CHARMm parameter set PARM21. It should be noted that this method of probing the channel for potential liganding sites is closely related to the GRID program of Goodford (1985) and to the method of Furois-Corbin and Pullman (1986).

Ion-channel interaction energies are evaluated as the difference between the energy with the ion at a given point and the energy when ion and channel are separated by a

considerable distance (typically ≥ 50 Å). Energy profiles are generated by translating the ion along the pore (i.e. z) axis, the interaction energy being evaluated as a function of z.

Results

M2 *sequences*

The sequences of several M2 regions are given in the first half of Table 1. They are of: the four subunits of the *Torpedo* nAChR (nAChR-α etc.; Noda et al. 1983); a kainate (i.e. glutamate) receptor channel (GluR-1; Hollman et al. 1989); the NMDA-R (Moriyoshi et al. 1991); the $5HT_3$-R (Maricq et al. 1991); three $GABA_A$-R subunits (Schofield et al. 1987; Pritchett et al. 1989); and a Gly-R subunit (Grenningloh et al. 1987). The ion selectivities (anion vs. cation) of the corresponding channels are noted. The numbering scheme at the top of Table 1 refers to the *Torpedo* nAChR-α sequence. Thus the M2 region shown runs from residue E259 (the "intermediate ring") to one residue past residue E280 (the "extracellular ring"). These two rings of anionic residues have been implicated in ion selectivity of the nAChR (Konno et al. 1991). The numbering scheme used throughout the remainder of this paper is defined at the bottom of the table. This refers to the positions within the M2 helix, and thus is independent of any particular receptor subunit sequence.

The hydroxylated sidechains believed to line the central pore are underlined in Table 1. Mutagenesis experiments have implicated residues at positions 4 (Villaroel et al. 1991; Imoto et al. 1991), 8 and 12 (Leonard et al. 1988; Charnet et al. 1990) in ion-channel interactions. It can be seen that these residues are strongly conserved. Residue 4 is generally T or S (more rarely G, A or V), residue 8 is generally S or T (rarely A), and residue 12 is generally A, S or T (rarely G). It should also be noted that in the anion channel sequences, residues 8 and 12 are T rather than S.

On the basis of the above conserved features simplified M2 sequences were designed, given in the lower part of Table 1 (*p2* to *p6*). The aim of these models is to explore the properties of the central region of the putative ion channel i.e. that between the selectivity filters defined by the intermediate (position 1) and extracellular rings (position 22) of anionic residues. In these models the helix was extended one residue beyond the extracellular ring, to position 23. A synthetic 23-mer peptide corresponding to the *Torpedo* nAChR-δ sequence forms cation selective channels in planar bilayers (Oiki et al. 1988). Furthermore, it transpires (see below) that the results obtained are not strongly dependent upon the exact length of the M2 model. In order to focus on the "4–8–12" motif, all other residues are alanines. Model *p2* has serine residues at positions 4, 8 and 12, whereas model *p3* has threonine residues. Model *p2'* is a truncated version of *p2* (15 residues rather than 23). Models *p4*, *p5* and *p6* are intended to represent the 4–8–12 motifs in the *Torpedo* nAChR α, β/δ and γ subunits respectively.

Model M2 helices (for *p2* to *p6*) were constructed with the backbone in a right-handed α-helical conformation (Arnott and Wonnacott 1966), and subjected to at least 50 cycles of steepest descents energy minimization. This resulted in only minor changes to the backbone conformation, mainly at the N- and C-termini. Atomic charges were assigned according to the CHARMm parameter set. The N- and C-termini were set to be in their uncharged forms. Initially, the S and T sidechains were set in their extended (i.e. $\chi_1 = t$, $\chi_2 = t$) conformations (see Fig. 1 A).

Table 1. Sequences of M2 helices

Channel	Ion	Sequence
		262 266 270
nAChR-α	cation	E-K-M-T-L-S-I-S-V-L-L-S-L-T-V-F-L-L-V-I-V-E-L
nAChR-β	cation	E-K-M-S-L-S-I-S-A-L-L-A-V-T-V-F-L-L-L-L-A-D-K
nAChR-γ	cation	Q-K-C-T-L-S-I-S-V-L-L-A-Q-T-I-F-L-F-L-I-A-Q-K
nAChR-δ	cation	E-K-M-S-T-A-I-S-V-L-L-A-Q-A-V-F-L-L-L-T-S-Q-R
GlurR-1	cation	N-E-F-G-I-F-N-S-L-W-F-S-L-G-A-F-M-Q-Q-G-C-D-I
NMDA-R	cation	D-A-L-T-L-S-S-A-M-W-F-S-W-G-V-L-L-N-S-G-I-G-E
$5HT_3$	cation	E-R-V-S-F-K-I-T-L-L-L-G-Y-S-V-F-L-I-I-V-S-D-T
$GABA_A$-R-α	anion	A-R-T-V-F-G-V-T-T-V-L-T-M-T-T-L-S-I-S-A-R-N-S
$GABA_A$-R-β	anion	A-R-V-A-L-G-I-T-T-V-L-T-M-T-T-I-S-T-H-L-R-E-T
$GABA_A$-R-γ^2	anion	A-R-T-S-L-G-I-T-T-V-L-T-M-T-T-L-S-T-I-A-R-K-S
Gly-R-α	anion	A-R-V-G-L-G-I-T-T-V-L-T-M-T-T-Q-S-S-G-S-R-A-S
p2		A-A-A-S-A-A-A-S-A-A-A-S-A-A-A-A-A-A-A-A-A-A-A
p2'		A-A-A-S-A-A-A-S-A-A-A-S-A-A-A
p3		A-A-A-T-A-A-A-T-A-A-A-T-A-A-A-A-A-A-A-A-A-A-A
p4		A-A-A-T-A-A-A-S-A-A-A-S-A-A-A-A-A-A-A-A-A-A-A
p5		A-A-A-S-A-A-A-S-A-A-A-A-A-A-A-A-A-A-A-A-A-A-A
p6		A-A-A-T-A-A-A-S-A-A-A-A-A-A-A-A-A-A-A-A-A-A-A
		4 8 12

In the models, *p2* to *p6*, the N and C terminal groups are in their uncharged forms, i.e. H_2N- and CO_2H respectively. The numbering at the top of the table corresponds to that of the *Torpedo* nAChR-α sequence. The numbering at the bottom corresponds to that used in this paper. For other details, see main text

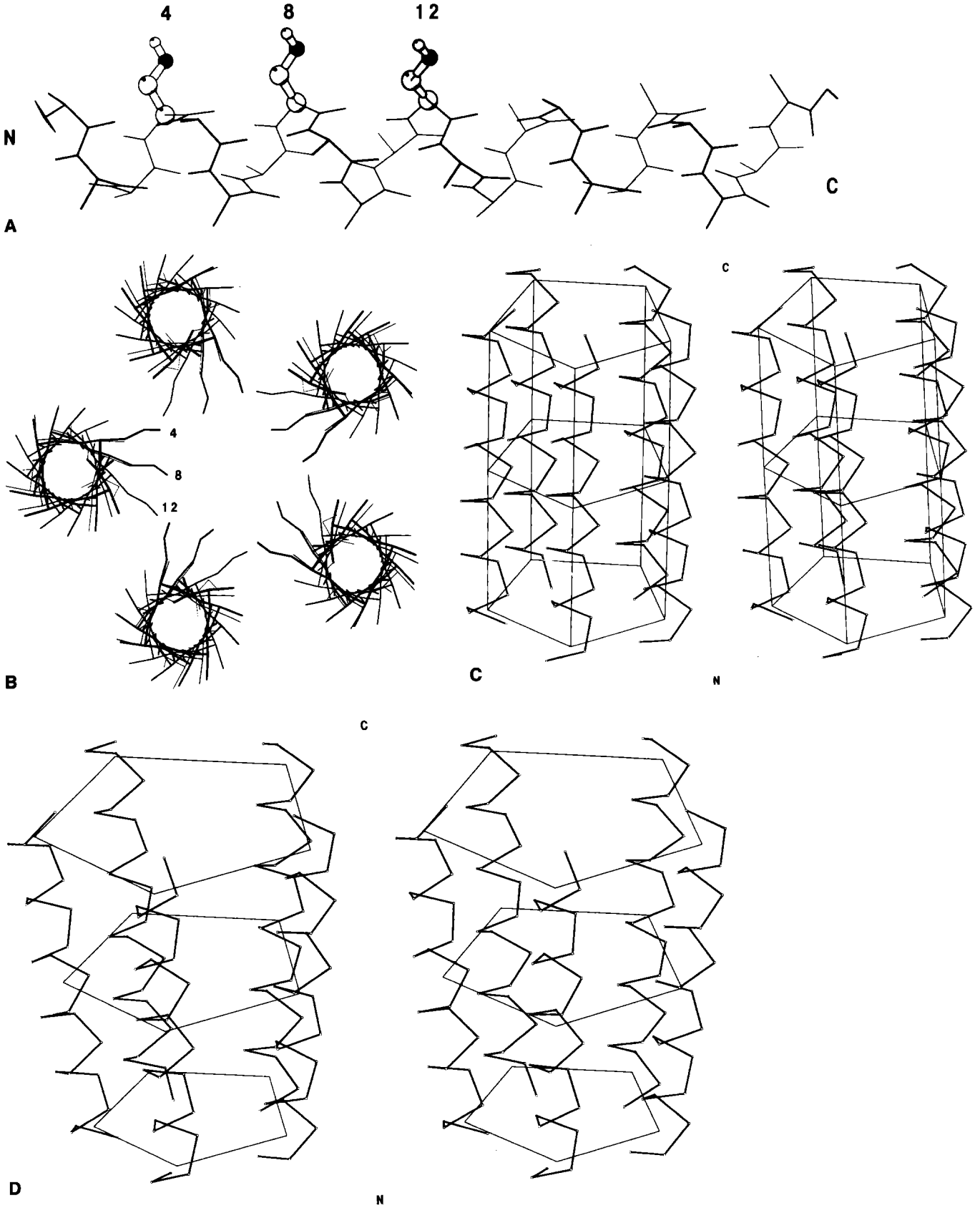

Fig. 1 A–D. Illustration of the model building procedure using a *p2t* helix. (**A**) shows the helical monomer. The N- and C-termini are labelled, as are the positions of residues S4, S8 and S12. (**B**) depicts a *p2t* helix bundle, viewed down the *z*-axis (i.e. down the axis of the central pore). The sidechains of S4, S8 and S12 of helix A are labelled. (**C**) and (**D**) are stereo pairs illustrating the geometries of packing parallel- and tilted-helix models respectively. In both diagrams, the helices are represented by Cα atom traces. Three dummy atoms are defined for each helix: D1 at the midpoint of Cα atoms of residues 1 to 4, D2 at the midpoint of Cα atoms of residues 1 to 23, and D3 at the midpoint of Cα atoms of residues 20 to 23. These dummy atoms may be employed to construct three pentagons which describe the overall shape of the bundle. (C) shows a bundle of parallel helices, as in *p2to5* etc. (D) shows a bundle in which each helix is tilted relative to the *z*-axis ($\Omega = 7°$, see text for details), as in *p2to5o* etc.

Helix bundles

The procedure for generation of helix bundles is illustrated using the *p2* monomer with its S sidechains in the extended, i.e. $\chi_1 = t$, conformation (*p2t* – see below). The sidechains of residues 4, 8 and 12 lie on the same face of the helix (Fig. 1 A). A parallel, $N = 5$, helix bundle was generated after rotating the monomer through $\theta = +20°$ such that the face of the helix defined by the Cα atoms of S4, S8 and S12 was directed along the *x*-axis. The interaxial separation of the helices was $R = 10$ Å. A space-filling model of the bundle showed that this placed the helices in close contact without any atomic overlaps. These parameter values were employed in all subsequent models of parallel-helix bundles. Viewing the resultant model down the *z*-axis (Fig. 1 B) shows that the sidechains of S4, S8 and S12 are directed towards the central pore.

Two classes of model were explored. Those with parallel helices were constructed as above, resulting in the bundle geometry illustrated in Fig. 1 C. If for each helix three dummy atoms are defined, D1 at the midpoint of Cα:1–4, D2 at the midpoint of Cα:1–23 and D3 at the midpoint of Cα:20–23, then three pentagons may be constructed to describe the overall shape of the bundle. For the parallel-helix bundle the three pentagons are almost identical, with D1-D1 = 9.7 Å, D2-D2 = 9.9 Å, and D3-D3 = 10.0 Å.

The second class of model constructed had their helices tilted relative to the *z*-axis by an angle of $\Omega = +7°$ (Fig. 1 D). This value was selected in order to generate a model comparable to that constructed by Furois-Corbin and Pullman (1989a), the dimensions of which the authors selected so as to permit access of the open-channel blocker and photoaffinity label chlorpromazine (CPZ) to residues 8 and 11. The interaxial separation at the centre of the helices (defined by the midpoint of Cα:1–23) was set to $R = 12.4$ Å. As before, one may construct three pentagons to describe the overall geometry of the bundle. The bundle is narrower at the N-termini than at the C-termini: D1-D1 = 10.1 Å, D2-D2 = 12.4 Å, and D3-D3 = 14.4 Å. Site-directed mutagenesis studies suggest that the nAChR pore is constricted close to the N-termini of the M2 helices (Imoto et al. 1991; Konno et al. 1991).

The two classes of models, parallel and tilted, were used in all subsequent studies. In both models it as assumed that the M2 helix bundle is pentameric and approximately parallel, as supported by the biochemical and structural evidence.

Sidechain conformations

In order to explore possible interactions of S and T sidechains with permeant ions, it is necessary to consider in some detail possible conformations of these sidechains. Sidechain conformations are defined by two torsion angles: $\chi_1 = N{-}C\alpha{-}C\beta{-}O\gamma$ and $\chi_2 = C\alpha{-}C\beta{-}O\gamma{-}H\gamma$. Thus χ_1 determines the locations of the non-hydrogen atoms of the sidechain, and χ_2 fixes the position of the terminal Hγ.

Table 2. Sidechain conformations of monomers

Model	χ_1	χ_2/°		
		4	8	12
p2to	*t*	+ 50	− 25	− 70
p2th	*t*	−145	+165	+ 95
p2gpo	*g*+	− 70	+ 70	+ 80
p2gph	*g*+	−160	−160	−160
p2gmo	*g*−	+ 36	− 65	− 80
p2gmh	*g*−	+145	+175	−150
p3gpo	*g*+	− 70	+ 65	+ 75
p3gph	*g*+	−165	−170	−175
p3gmo	*g*−	+ 45	− 70	− 80
p3gmh	*g*−	+150	+175	−100

The sidechain torsions angles are defined as follows: $\chi_1 = N{-}C\alpha{-}C\beta{-}O\gamma$ and $\chi_2 = C\alpha{-}C\beta{-}O\gamma{-}H\gamma$. For χ_1, the three conformers are defined as: *t*, $\chi_1 = 180°$; *g*−, $\chi_1 = +60°$; and *g*+, $\chi_1 = -60°$

Gray and Matthews (1984) examined the χ_1 values of S and T residues located in helices. They showed that for S residues, χ_1 could adopt values typical of either the *g*−, *t*, or *g*+ conformations (centred about $\chi_1 = +60°$, 180° and −60° respectively). The *g*− and *g*+ conformations were somewhat favoured over *t* as they permitted hydrogen bonding from Hγ:n to O:(n−3) and/or O:(n−4) (see also Baker and Hubbard 1984). T residues were shown to adopt mainly the *g*− and *g*+ conformations, as a result of a steric clash between Cγ:n and O:(n−3) when $\chi_1 = t$.

On the basis of these stereochemical constraints, helices have been constructed (see Table 2) for *p2* with $\chi_1 = g-$ (*p2gm*...), *t* (*p2t*...) or *g*+ (*p2gp*...), and for *p3* with $\chi_1 = g-$ (*p3gm*...) or *g*+ (*p3gp*...), thus defining the positions of the non-hydrogen atoms of the S/T sidechains. Clearly the χ_2 values (i.e. the positions of the Hγ atoms) have a major influence on potential interactions of M2 helices with permeant ions. Accordingly, a conformational search procedure was employed which permitted "optimization" of χ_2 values for a given species of permeant ion, so as to maximize possible channel-ion interactions.

The conformational search procedure is illustrated in Fig. 2, for residue T8 of helix *p3gm* (i.e. monomer *p3* with $\chi_1 = g-$). The empirical energy of the monomer was evaluated as a function of χ_2, using a torsion angle increment of $\Delta\chi = 5°$. These case were considered: (A) a *p3gm* helix in isolation; (B) a *p3gm* helix taken from a parallell-helix bundle with a K^+ ion placed on the *z*-axis level with the Oγ atom of T8 (at $z = -7.55$ Å); and (C) a *p3gm* helix with a Cl^- ion at $z = -7.55$ Å. Thus in (B) and (C) the ion is in its position of closest approach to Oγ:8 as it moves along the central axis of a parallel-helix bundle. The resultant energy vs. χ_2 curves are given in Fig. 2 D. Note that the energies have been normalised so that $E = 0$ for $\chi_2 = 0°$.

For the *p3gm* helix on its own (Fig. 2 D; curve A) three energy minima are seen, corresponding to $\chi_2 = +70°$, +170° and −80° (+280°) i.e. the *g*−, *t* and *g*+ conformations respectively. Of these, $\chi_2 = -80°$ is the most stable conformation and is shown in Fig. 2 A. It can be seen

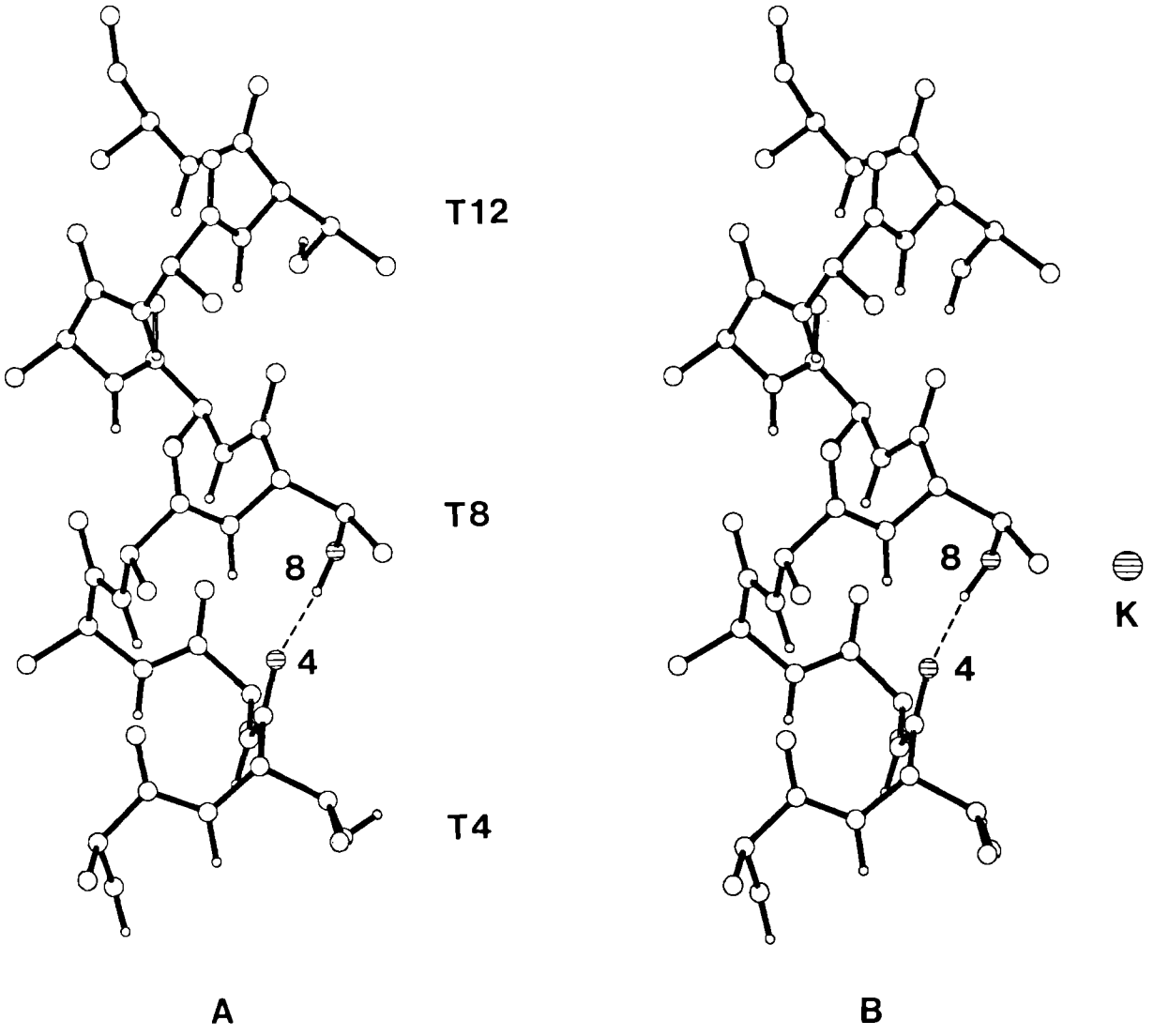

Fig. 2 A–D. The method employed to "optimize" the values of $\chi_2 = C\alpha-C\beta-O\gamma-H\gamma$, exemplified for residue T8 of helix *p3gm*. In (**A**) the lowest energy conformation from a grid search on χ_2 of T8 ($\Delta\chi = 5°$) is shown. The T4, T8 and T12 sidechains are labelled and oxygen atoms Oγ:8 and O:4 are shaded. It can be seen that, in the absence of any ion, χ_2 is such that Hγ:8 can form a hydrogen bond to O:4 (broken line; see Table 3 and text). (**B**) is the equivalent diagram illustrating the result of a χ_2 search conducted in the presence of a K^+ ion. The *p3gm* helix occupied the position it would in a parallel helix bundle ($\theta = 20°$, $R = 10$ Å – see text), with the ion placed on the *z*-axis level with Oγ:8. The minimum energy conformation depicted is similar to that in (A), with a hydrogen bond (broken line) from Hγ:8 to O:4. (**C**) shows the minimum energy conformation when the K^+ ion is replaced by Cl^-. Hγ:8 is oriented towards the Cl^- ion, pointing away from O:4. (**D**) depicts potential energy vs. χ_2 curves for the cases considered in A, B and C. For A, the minimum is at $\chi_2 = -80°$, i.e. approximately $g+$; for B, the minimum is at $\chi_2 = -70°$, i.e. approximately $g+$; whereas for C, the minimum is at $\chi_2 = 175°$, i.e. approximately t

that this conformation is such that a hydrogen bond is formed from Hγ:8 to O:4, in agreement with the analysis of Gray and Matthews (1984).

The result when a K^+ ion is present is shown in curve B of Fig. 2D. There is a broad energy maximum corresponding to the $\chi_2 = t$, arising from electrostatic repulsion between Hγ:8 and K^+. There is an energy minimum at $\chi_2 = -70°$. The corresponding structure is shown in Fig. 2B. As before, a hydrogen bond is formed between Hγ:8 and O:4. Consequently, the lone pair electrons of Oγ:8 are directed towards the K^+ ion.

A markedly different minimum energy conformation is found when a Cl^- ion is present (Fig. 2C, curve D). There is a deep energy minimum at $\chi_2 = +175°$. This results in Hγ:8 being directed towards the Cl^- ion, and hence a hydrogen bond to O:4 is not formed. Thus it can be seen that electrostatic interactions between permeant ion and sidechain Hγ atom determine the preferred conformation of that sidechain.

The above procedure was used to define sidechain conformations for helices in cation and anion selective channel models. For example, a K^+ ion was placed adjacent to helix *p2t*. It was positioned on *z* level with Oγ:4, Oγ:8 and Oγ:12 (successively), and the minimum energy conformations obtained by conformational searches on χ_2 were selected in order to generate helix *p2to* (i.e.

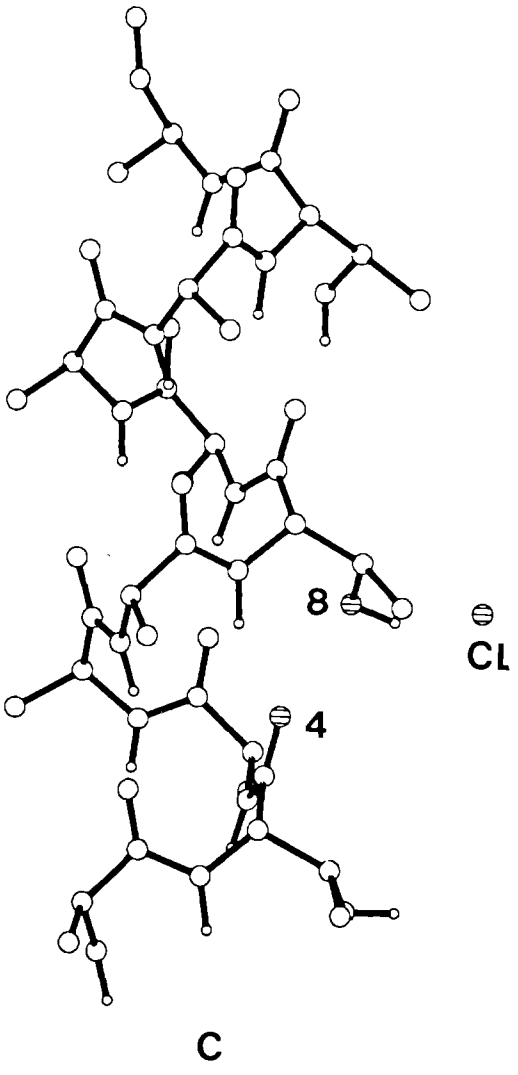

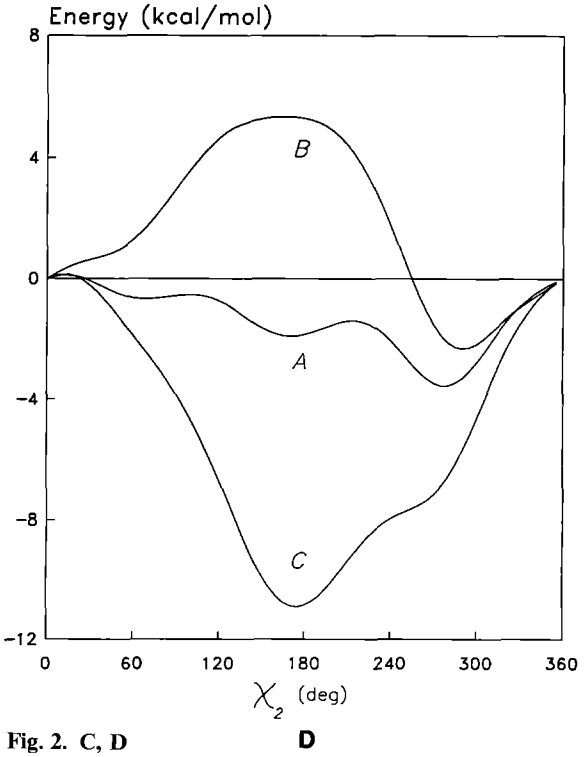

Fig. 2. C, D

monomer *p2*, $\chi_1 = t$, Oγ atoms of 4, 8 and 12 directed towards the permeant ion). Repeating this procedure with a Cl^- ion yielded helix *p2th*, with the Hγ atoms directed towards the central ion. This procedure was repeated for *p2t* through to *p3gm* to generate the helices defined in Table 2. It can be seen that these fall into two classes. For "*o*" models (i.e. ion = K^+) the χ_2 values are clustered around $g+$ and $g-$, whereas for "*h*" models (i.e. ion = Cl^-) χ_2 is clustered around the *t* conformation. In the "*o*" models the Hγ atoms are directed away from the permeant ion, whereas in the "*h*" models they point towards the permeant ion.

Hydrogen bonding patterns of model helices are given in Table 3. The criteria for hydrogen bond formation were based on those described by Baker and Hubbard (1984), with a maximum O···H distance of 2.5 Å and a minimum value of the angle C−Ô···H of 90°. No hydrogen bonding is found in the *p2t* helices (in agreement with Gray and Matthews, 1984) or in the "*h*" helices (with the exception of T12 of *p3gmh*). Hydrogen bonding, both Hγ:n···O:(n−4) and (less frequently) Hγ:n···O:(n−3) is seen in the *p2gp*, *p2gm*, *p3gp* and *p3gm* "*o*" helices. This is most extensive in *p2gmo* in which Hγ:8 forms a bifurcated hydrogen bond to both O:5 and O:4.

Overall, it is evident that the minimum energy conformation around χ_2 is determine by the balance between hydrogen bond formation to preceding mainchain carbonyl atoms, and electrostatic interactions with the nearby ion. Hydrogen bonds are formed when a cation is present, but not when an anion is present. Interestingly there appear to be no significant differences between the conformations adopted by the corresponding *p2* and *p3* helices.

Ion profiles and helix dipoles

The energy profile for an ion is obtained by translating the ion along the central axis of the pore, evaluating the channel-ion interaction energy as a function of *z*. As discused by Furois-Corbin and Pullman (1989 b) and by Eisenman and Alvarez (1991), with a channel formed by a bundle of parallel, or approximately parallel, helices, this energy profile is dominated by the effect of the aligned helix dipoles. The latter may be approximated by charges of +1/2 at the N-termini and of −1/2 at the C-termini of the helices (Hol et al. 1978). However, there are several reasons for believing that such interactions are of much lesser importance in intact receptor-channel proteins. Eisenman and Alvarez (1991) have shown that the presence of rings of charged sidechains at the mouth of the pore cancels the helix dipole effect in a nAChR M2δ helix bundle model. Furois-Corbin and Pullman (1989 b) suggest that in the intact nAChR presence of an outer bundle of M1 or M3 helices cancels the helix dipole effect as a result of a bundle of dipoles pointing in the opposite direction. In the current study the focus is on the 4-8-12 motif and channel-ion interactions when the ion is within the pore. Thus a method for subtracting the helix dipole effect has been devised.

Table 3. Sidechain-mainchain hydrogen bonding of monomers

Models	Sidechain	d/Å					
				"o" Models (K^+)		"h" Models (Cl^-)	
		Oγ–O:(n–3)	Oγ–O:(n–4)	Hγ–O:(n–3)	Hγ–O:(n–4)	Hγ–O:(n–3)	Hγ–O:(n–4)
p2to	4	5.0	–	5.7	–	5.2	–
&	8	5.1	4.7	5.4	5.4	5.5	4.8
p2th	12	5.1	4.8	5.1	5.4	5.9	5.0
p2gpo	4	4.8	–	5.6	–	5.3	–
&	8	4.8	2.9	4.4	2.0*	5.4	3.5
p2gph	12	4.8	2.9	4.4	2.0*	5.4	3.5
p2gmo	4	3.0	–	2.4*	–	3.6	–
&	8	3.0	3.1	2.4*	2.2*	3.6	3.4
p2gmh	12	3.0	3.1	2.6	2.2*	3.5	2.9
p3gpo	4	4.9	–	5.7	–	5.4	–
&	8	4.9	3.0	4.5	2.1*	5.4	3.5
p3gph	12	4.9	4.0	4.5	2.1*	5.3	3.4
p3gmo	4	3.1	–	2.7	–	3.8	–
&	8	3.1	3.1	2.7	2.1*	3.8	3.5
p3*gmh*	12	3.1	3.1	2.8	2.1*	3.1	2.2*

Hydrogen bonds are indicated by a*. Criteria for hydrogen bond formation were based upon those of Baker and Hubbard (1984), as described in the main text

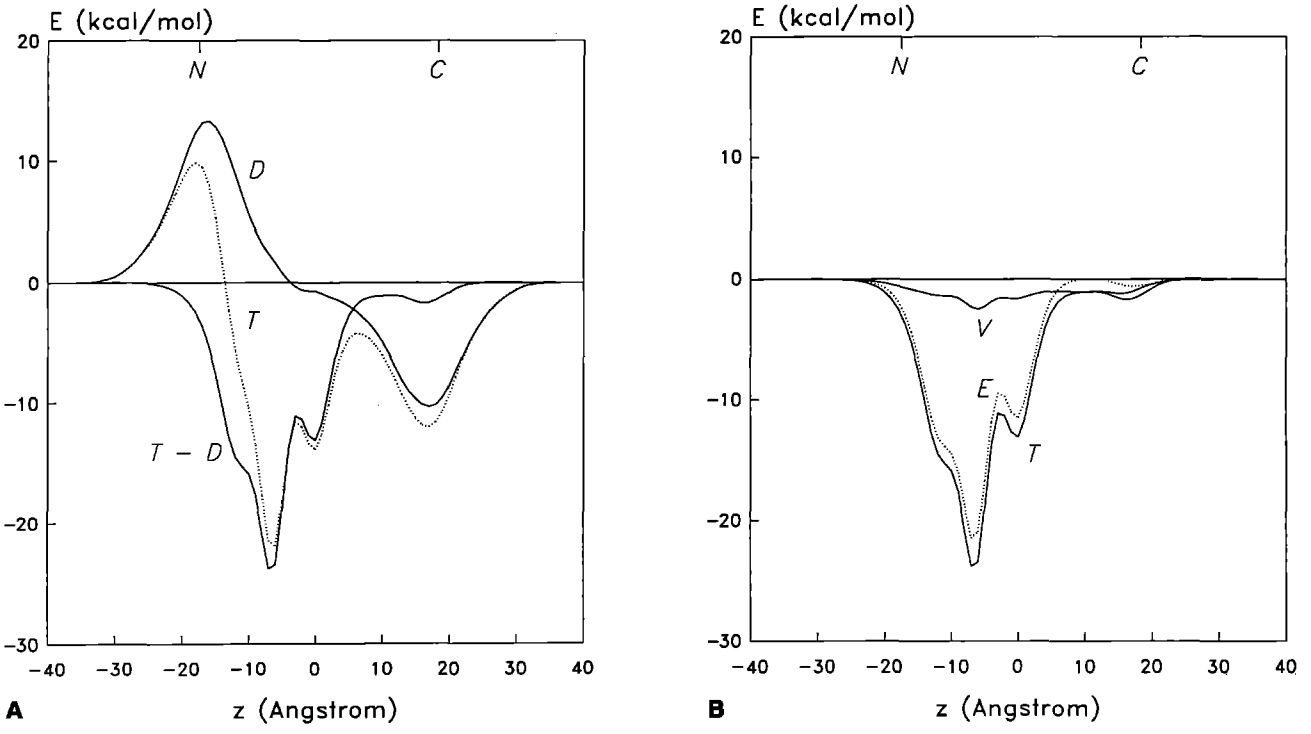

Fig. 3. (**A**) is an illustration of the procedure used to "subtract" the effect of helix dipoles on K^+-ion profiles. Curve T (dotted line) shows the K^+-profile for model *p2to5* (see text), i.e. the interaction energy between the ion and the helix bundle as a function of distance along the pore axis (*z*). This profile contains contributions both from aligned helix dipoles of the bundle and from polar sidechains of the 4-8-12 motif. N and C indicate the approximate positions on the *z*-axis of the N- and C-termini of the helices. Curve D shows the corresponding electrostatic energy profile for model *p0n5*, i.e. for a parallel bundle of polyalanine helices with the same packing geometry as *p2to5*. This profile contains only the contribution from the helix dipoles. Curve T–D is the profile generated by the difference between profiles T and D. T–D reveals interactions between the ion and sidechains of *p2to5*, unobscured by the helix dipole effect. It is the latter type of profile, with the helix dipole effect subtracted, which is used in the remainder of the paper. (**B**) shows the K^+ profile for model *p2to5* broken down into its component terms, i.e. E_V (V), E_E (E, dotted line), and E_T (T). Note that the helix dipole effect has been subtracted from E and T

The K^+ ion profile for model *p2to5* (i.e. a parallel bundle of five *p2to* helices) is shown as curve T in Fig. 3A. This profile includes the helix dipole contribution. It can be seen that there is an energy maximum at $z = -18$ Å corresponding to the N-termini of the helices, and a minimum at $z = +17$ Å, corresponding to the C-termini. These reflect the interaction of the ion with the aligned helix dipoles and so, to some extent, interactions of the ion with the 4-8-12 motif are obscured.

The corresponding K^+ ion profile for model *p0n5* is shown in curve D of Fig. 3A. Model *p0n5* is made up of five polyalanine (A_{23}) helices, and has the same bundle geometry as *p2to5*. As there are no polar sidechains in *p0* this profile is entirely due to backbone i.e. helix dipole interactions. In evaluating the *p0n5* profile *only* the electrostatic energy, E_E, is employed. If one subtracts the *p0n5* interaction energy profile from the *p2to5* energy profile, curve T–D (Fig. 3A) is obtained. This reveals interactions between the ion and the sidechains, unobscured by the helix-dipole contribution. The maximum at $z = -18$ Å and the minimum at $z = +17$ Å are thus removed.

This procedure is used throughout the remainder of this paper, i.e. for model X the interaction energy is defined by:

$$E_T(X) = E_V(X) + E_E(X) - E_E(p0)$$

where $E_E(p0)$ represents the helix dipole term, given by the electrostatic interaction energy of the corresponding *p0* (i.e. polyalanine) model.

It is useful to examine the relative contributions of the van der Waals and electrostatic components to the overall interaction energy. This is done in Fig. 3B, again for model *p2to5* with a K^+ ion probe. The solid curve, V, represents the van der Waals energy and the dotted curve, E, the electrostatic energy. Curve T is the total interaction energy. Note that the helix dipole contribution has been subtracted from both E and T. It is evident that although there is a weak favourable van der Waals interaction whilst the ion is within the pore, the overall interaction energy is dominated by the electrostatic term. Inspection of the E_V and E_E components reveals that this is the case for all of the models discussed in this paper.

Parallel-helix models

Ten parallel-helix models were constructed. It is useful to define the nomenclature used subsequently to refer to these. Thus, *p2to5* is a bundle of $N = 5$ parallel *p2* helices with $\chi_1 = t$ and χ_2 in the "*o*" (i.e. ion = K^+) conformation. Likewise, *p2to5* is made up of five *p2* helices with $\chi_1 = g+$ and χ_2 in the "*o*" conformation. Table 4 lists the ten models thus defined.

p2 Bundles, K^+ ion probe. K^+ ion profiles for the three *p2"o"* models are given in Fig. 4A: (T) *p2to5*; (P) *p2gpo5*; and (M) *p2gmo5*. The *p2to5* profile has two distinct minima, at $z = -7$ Å and $z = 0$ Å, along with a shoulder at ca. $z = -11$ Å. These correspond to the Oγ atoms of residues S8 ($z = -6.0$ Å), S12 ($z = +0.1$ Å) and S4 ($z = -12.0$ Å) respectively. Of these minima, the deepest is that associated with S8. The *p2gpo5* profile shows minima in the same three positions. Those corresponding to S4 and S8 are not as deep as in the previous case, but that corresponding to S12 is somewhat deeper. The profile for *p2gmo5* shows a well-defined energy minimum at S4, a shoulder at S8 and a small barrier at S12.

These features can be explained by examination of the corresponding structures (Fig. 5A–C), and by measurement of closest approach distances as the K^+ ion is translated along z (Table 4). Thus, in model *p2to5* the Oγ:8 atoms point directly towards the central axis of the pore (Fig. 5A), and the Oγ–K approach distance is closer for S8 than for S4 or S12. S8 thus generates the strongest interactions with the K^+ ion. For model *p2gpo5*, Oγ:12 points more directly towards the pore axis (Fig. 5B) and the Oγ–K approach distance is closer for S12 than for S4 or S8. However, the approach distances for *p2gpo5* are greater than those for *p2to5* – hence the overall deeper minima for the latter model. The weaker interactions for *p2gmo5* can be understood in terms of more distant Oγ–K approaches and, in the case of S12, the Oγ atoms being directed away from the central axis (Fig. 5C).

p2 Bundles, Cl^- ion probe. The corresponding Cl^- ion profiles for the three *p2"h"* models are given in Fig. 4B. The *p2th5* profile (curve T) has three distinct energy minima (at $z = -12$, -7 and 0 Å), corresponding to residues S4, S8 and S12 respectively. The *p2gph5* profile (curve P) has a pronounced minimum corresponding to S8, with lesser minima at S4 and S12. The *p2gmh5* profile is similar, but the S4 and S8 minima are of approximately equal depth. Once again, these features may be understood via inspection of the corresponding structures (Fig. 5D–F) and measurement of closest approach (Hγ–Cl) distances. In all three models the Hγ atoms are directed towards the centre of the pore. However, this is most pronounced for *p2th5*. The Hγ–Cl approach distances correlate well with the relative depths of the energy minima. It is interesting to note that for both the "*o*" and the "*h*" models the closest Oγ–K or Hγ–Cl approaches are obtained when χ_1 is in the t position.

p3 Bundles. The K^+ ion profiles for the two *p3"o"* models and the Cl^- ion profiles for the two *p3"h"* models are shown in Fig. 4C, D respectively. In both cases the profiles closely resemble those of the corresponding *p2* models. This can be seen (Table 4) to reflect similar closest approach distances to those for the *p2* models. Note that only $\chi_1 = g+$ or $g-$ models are explored for *p3*. As discussed above, the $\chi_1 = t$ conformation is stereochemically disallowed for T residues (in helices). Thus it may be seen that, as far as $\chi_1 = g+$ and $g-$ models are concerned, substitution of T for S does not substantially alter channel-ion interactions.

Tilted-helix models

The corresponding ten tilted-helix bundles, with $\Omega = 7°$, were also constructed. For example, *p2to5o* (terminal *o* for omega) was constructed from the same *p2to* monomer as model *p2to5*, but with the constituent helices tilted relative to the z-axis. Ion interaction energy profiles for the tilted-helix models are shown in Fig. 6, and closest

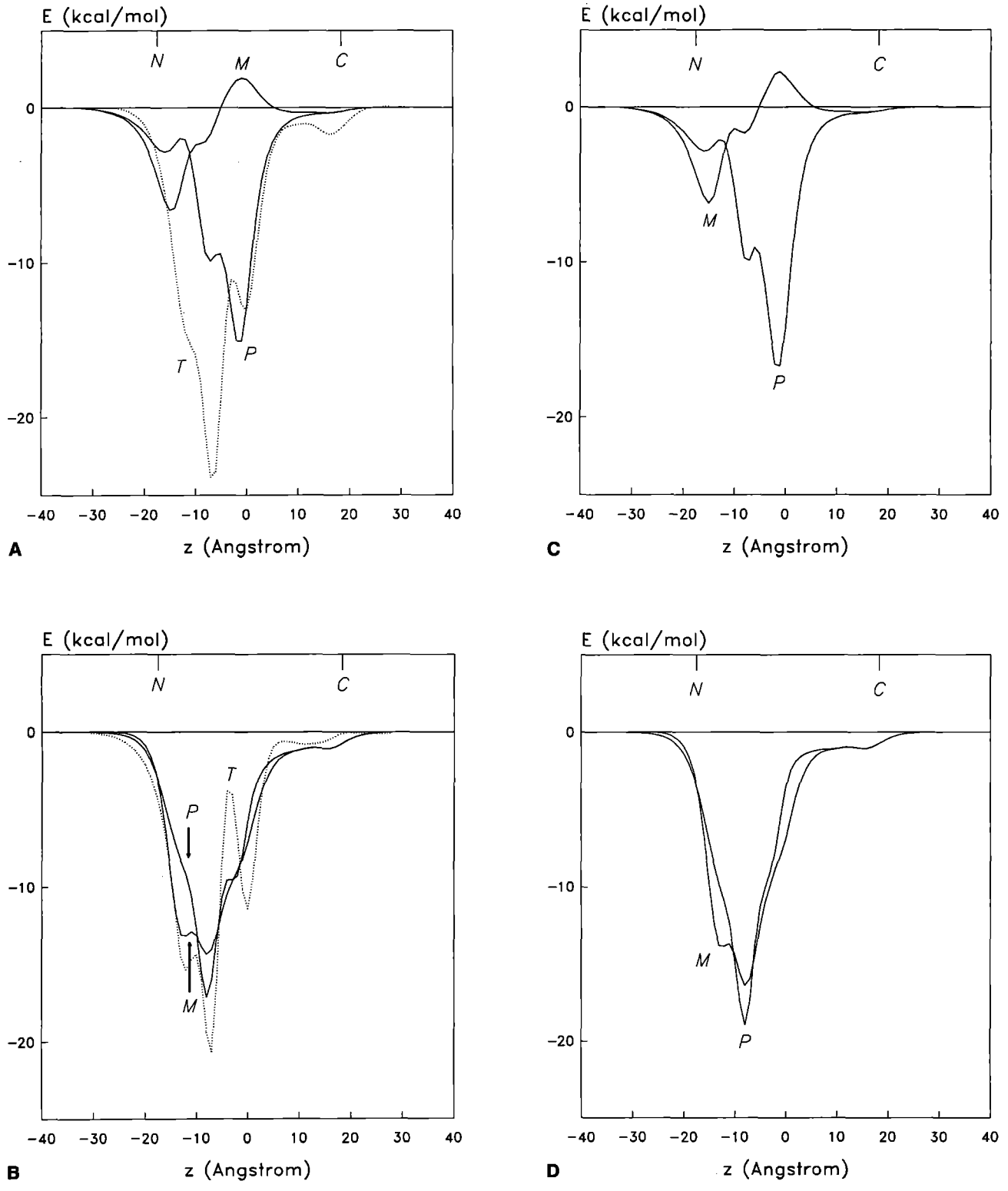

Fig. 4. Ion profiles for parallel-helix models formed from *p2* (**A** and **B**) and *p3* (**C** and **D**) helices. For all of the models the approximate positions on the *z*-axis of the N- and the C-termini are marked. (**A**) shows K^+-ion profiles for: T – *p2to5* (dotted line); P – *p2gpo5*; and M – *p2gmo5*. (**B**) shows Cl^- ion profiles for: T – *p2th5* (dotted line); P – *p2gph5*; and M – *p2gmh5*. (**C**) shows K^+-ion profiles for: P – *p3gpo5* and M – *p3gmo5*. (**D**) shows Cl^--ion profiles for: P – *p3gph5* and M – *p3gmh5*. In each case the corresponding *"p0n5"* profile has been subtracted (see Fig. 3A and text)

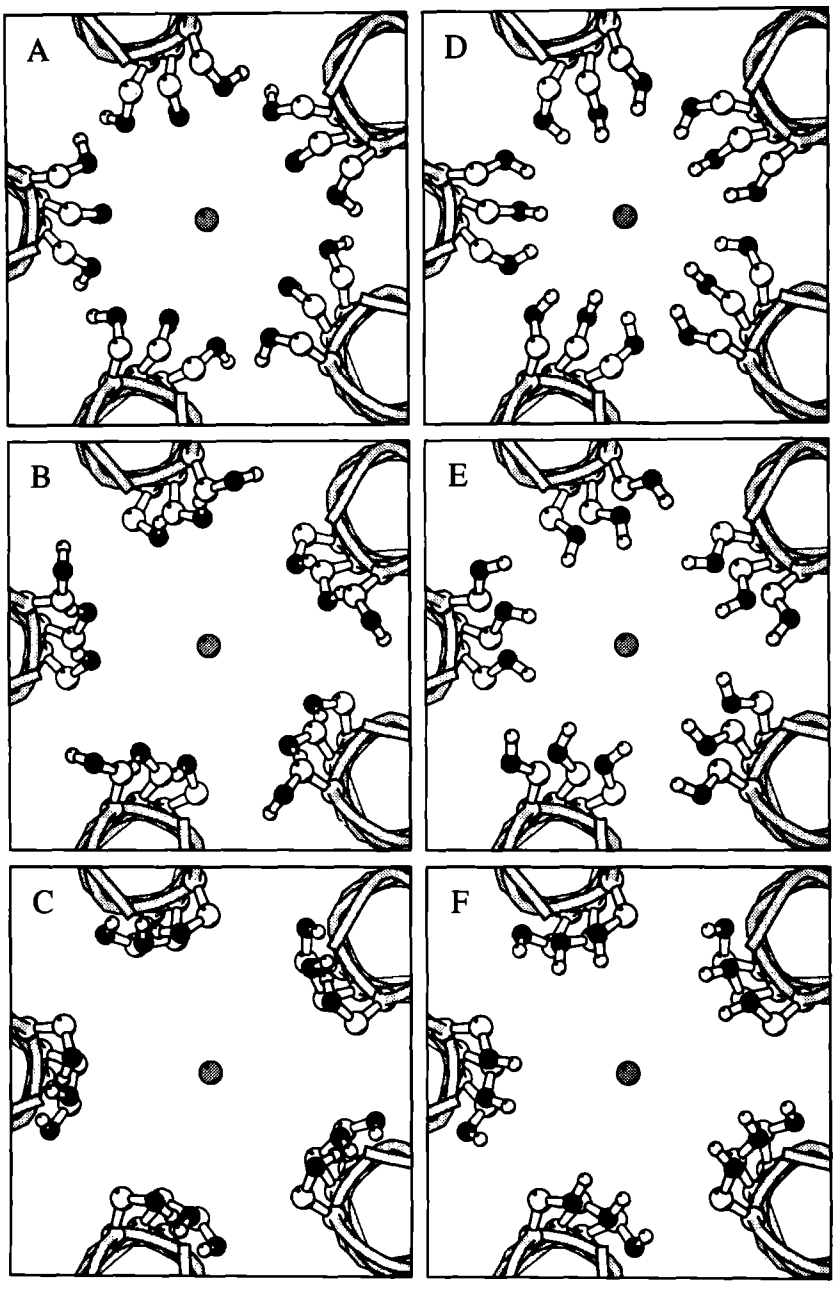

Fig. 5. *p2* helix bundles, viewed down the *z*-axis, showing residues in the vicinity of the 4-8-12 motif. The models shown are: (**A**) *p2to5*; (**B**) *p2gpo5;* (**C**) *p2gmo5;* (**D**) *p2th5;* (**E**) *p2gph5;* and (**F**) *p2gmh5*. In each case the permeant ion (K^+ in A, B and C; Cl^- in D–F) is shown a shaded circle. The backbone is shown as a shaded coil, the view being from the N-termini down the helices. The S4, S8 and S12 sidechains are shown in ball-and-stick fashion

approach distances are listed in the lower half of Table 4. Comparison of the corresponding profiles for parallel and tilted-helix bundles is illuminating. In general, tilting of the helices increases the closest approach distances, especially for residues 8 and 12. Consequently, the S/T4 interactions are largely unchanged but the S/T8 and S/T12 interactions are weakened. This leads to broader, shallower energy minima for the tilted-helix models. For example, if one compares the Cl^- profiles for *p2th5* (Fig. 4B; curve T) and for *p2th5o* (Fig. 6B; curve T) it is evident that for *p2th5* the deepest minimum corresponds to S8 whereas for *p2th5o* it corresponds to S4. Furthermore, all of the *p2th5o* minima are shallower than those for *p2th5*, particularly that corresponding to S12. Thus, one may conclude that changing the overall geometry of the helix bundle alters the details of the channel-ion interaction energy profiles, but that more general features remain unchanged.

Heteromeric bundle models

All of the models examined so far have possessed exact fivefold symmetry. However, although homomeric channels have been demonstrated to occur in vivo (e.g. the neuronal nAChR $\alpha 7$ channel; Couturier et al. 1990), many receptor-channels are known or believed to be heteromeric. For example, the *Torpedo* nAChR has stoichiometry $\alpha_2\beta\gamma\delta$. Consequently it is of interest to explore heteromeric bundle models using the techniques discussed above.

Helices *p4*, *p5* and *p6* were used to construct such models. As discussed above, these contain the 4-8-12

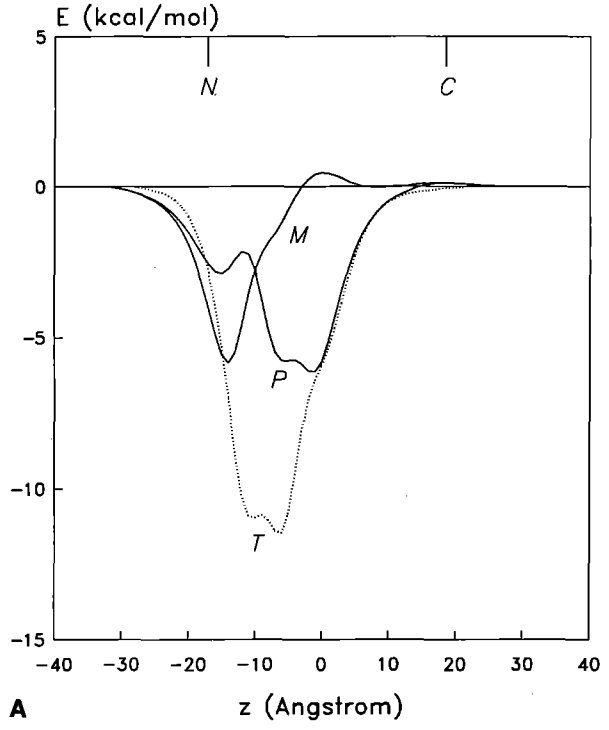

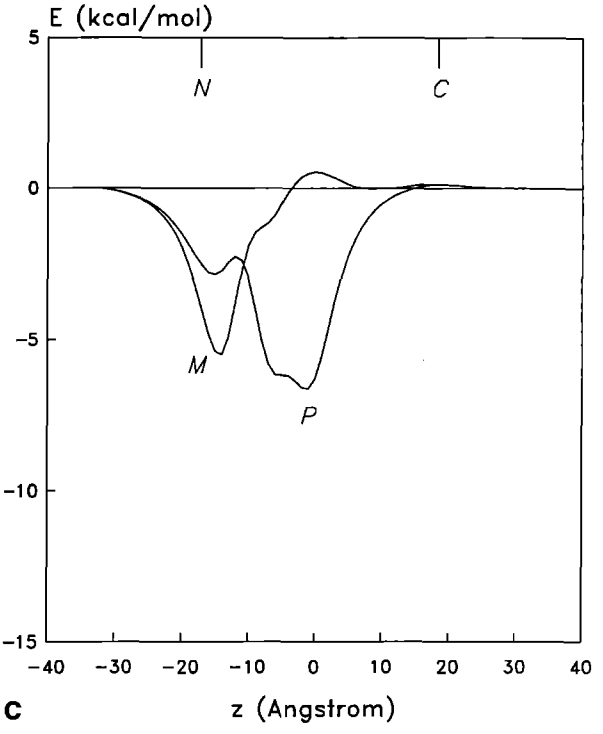

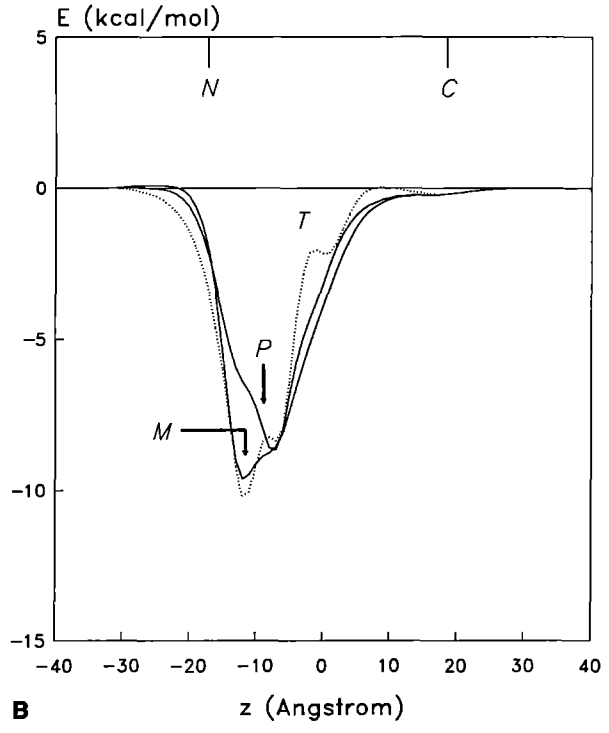

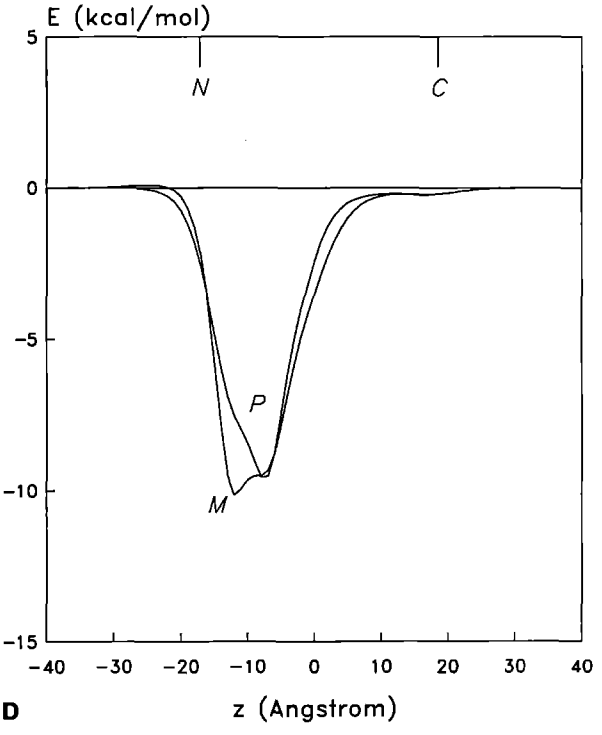

Fig. 6. Ion profiles for tilted-helix ($\Omega = 7°$) models formed from *p2* (**A** and **B**) and *p3* (**C** and **D**) helices. For all of the models the approximate positions on the *z*-axis of the N- and C-termini are marked. (**A**) shows K^+-ion profiles for: T – *p2to5o* (dotted line); P – *p2gpo5o;* and M – *p2gmo5o*. (**B**) shows Cl^- ion profiles for: T – *p2th5o* (dotted line); P – *p2gph5o;* and M – *p2gmh5o*. (**C**) shows K^+-ion profiles for: P – *p3gpo5o* and M – *p3gmo5o*. (**D**) shows Cl^--ion profiles for: P – *p3gph5o* and M – *p3gmh5o*. In each case the corresponding *"p0n5o"* profile has been subtracted (see text)

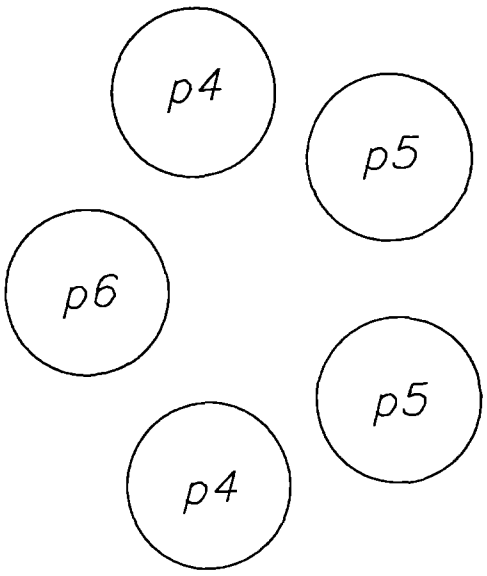

A

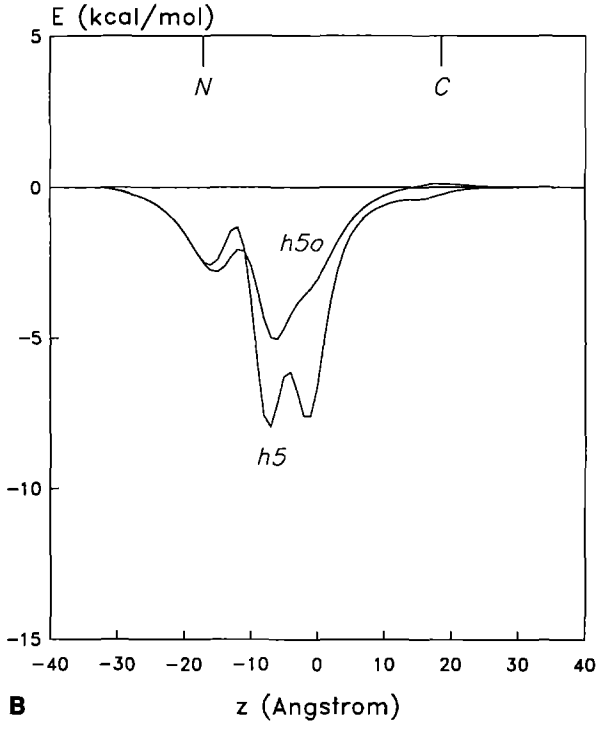

B

Fig. 7 A, B. A heteromeric bundle model (**A**) is a schematic diagram of the positions of the three helix types used to make up the pentameric bundle. (**B**) shows K^+ ion profiles for a parallel helix (*h5*) and a tilted helix (*h5o*, $\Omega = 7°$) model

motifs of *Torpedo* nAChR α, β/δ and γ subunits respectively. Although there is agreement as to the stoichiometry of *Torpedo* nAChR, the relative positions of subunits within the pseudo-symmetric pentamer remains the subject of some debate. Based on the model described by e.g. Galzi et al. (1991), heteromeric bundle models were constructed using the arrangement of monomers shown in

Table 4. Closest approach distances

Model	Side-chain	d(Oγ–K)/Å	Model	Side-chain	d(Hγ–Cl)/Å
p2to5	4	4.9	*p2th5*	4	4.0
	8	3.9		8	3.1
	12	4.7		12	3.7
p2gpo5	4	6.1	*p2gph5*	4	5.5
	8	4.7		8	3.8
	12	4.5		12	3.8
p2gmo4	4	5.2	*p2gmh5*	4	4.3
	8	5.4		8	4.7
	12	5.4		12	6.0
p3gpo5	4	6.2	*p3gph5*	4	5.5
	8	4.7		8	3.8
	12	4.4		12	3.9
p3gmo5	4	5.2	*p3gmh5*	4	4.3
	8	5.3		8	4.5
	12	6.3		12	6.2
p2to5o	4	6.5	*p2th5o*	4	5.8
	8	5.8		8	4.9
	12	6.3		12	5.6
p2gpo5	4	5.6	*p2gph5o*	4	4.7
	8	6.5		8	5.7
	12	8.2		12	7.7
p2gmo5o	4	5.4	*p2gmh5o*	4	4.5
	8	5.3		8	4.4
	12	6.7		12	5.8
p3gpo5o	4	6.6	*p3gph5o*	4	5.8
	8	5.8		8	4.9
	12	6.2		12	5.6
p3gmo5o	4	5.6	*p3gmh5o*	4	4.6
	8	6.4		8	5.6
	12	8.1		12	7.9

Fig. 7A. Sidechain conformations were set such that S residues had χ_1 and χ_2 values for the corresponding residues in *p2gpo* and T residues had χ_1 and χ_2 values for the corresponding residues in *p3gpo*. Thus, all χ_1 torsions were $g+$, χ_2 torsions were $g+$ for residue 4 and were $g-$ for residues 8 and 12. Two heteromeric bundle models were constructed – *h5* employing a parallel-helix bundle ($N = 5$, $\theta = +20°$, $R = 10$ Å), and *h5o* employing a tilted-helix bundle ($\Omega = +7°$).

K^+ ion profiles for *h5* and *h5o* are given in Fig. 7B. They should be compared with those for *p2gpo5*/*p3gpo5* (Fig. 4A, C) and for *p2gpo5o*/*p3gpo5o* (Fig. 6A, C) respectively. Considering *h5*, the energy minimum at $z = -16$ Å (corresponding to residue 4) is comparable to that seen for *p2gpo5*/*p3gpo5*. This reflects the presence of an S or T residue at position 4 in each of *p4*, *p5*, and *p6*. A similar situation holds for the energy minimum at $z = -7$ Å, corresponding to residue 8. However, the energy minimum at $z = -1$ Å is much shallower than the corresponding minima for *p2gpo5*/*p3gpo5*. Only *p4* has a hydroxylated residue at position 12 (S), whereas both *p5* and *p6* have A12. Thus the five Oγ:12 atoms of *p2gpo5*/*p3gpo5* are replaced by only two Oγ:12 atoms in *h5*, resulting in a weakened channel-ion interaction.

Turning to the K^+ ion profile for *h5o*, this bears a similar relationship to the profiles for *p2gpo5o*/*p3gpo5o*

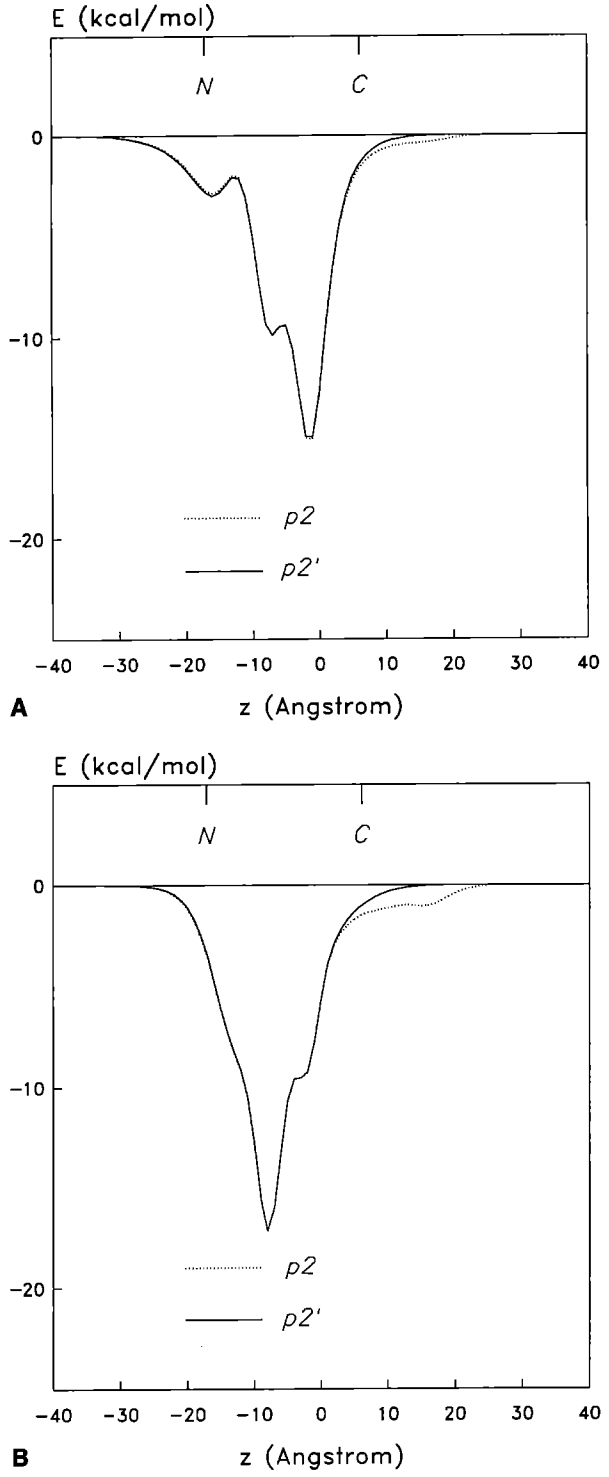

Fig. 8 A, B. Illustration of the effect of reducing the length of the helices on ion profiles. In (**A**) the K^+ ion profiles for models *p2gpo5* (dotted line; 23 residues) and *p2'gpo5* (15 residues) are illustrated. (**B**) depicts the Cl^- ion profiles for models *p2gph5* (dotted line) and *p2'gph5*

in that the energy minimum corresponding to residue 12 in the latter is reduced to a shoulder at ca. $z = 0$ Å for *h5o*. Overall, these results for heteromeric bundles suggest that the same general principles operate as for homomeric bundles, but that detailed ion profiles for channels will depend upon their subunit composition.

Truncated M2 *helix modles*

In all of the previous models it has been assumed that the M2 helices are 23 residues (i.e. ca. 35 Å) long. A length of 20–25 residues for a transmembrane helix is a common assumption as it would permit such a helix to span the central hydrophobic region of a lipid bilayer (Capaldi 1982). However, it is uncertain whether the M2 helices of e.g. the nAChR extend to this length. The site-directed mutagenesis studies cited earlier support residues 1, 4, 8 and 12 as forming the hydrophilic face of an M2 helix. However an M2 helix extending not much further than residue 12 would be as consistent with these results as would a longer one. Conservation of T15 for anion selective channels suggests that the M2 helix may be at least 15 residues long, although there is no mutagenesis data to support this. Although a 15-mer helix would not on its own span an undistorted bilayer, it should be born in mind that within the intact protein a bundle of such helices would be surrounded by other membrane spanning peptide chains, and so M2 helix-bilayer length mismatch need not be energetically unfavourable.

In view of these considerations, helix *p2'* was chosen as a 15-residue equivalent of *p2*. Monomers *p2'gpo* and *p2'gph* were constructed, with $\chi_1 = g+$ and χ_2 values as in *p2gpo* and *p2gph* respectively. K^+ and Cl^- ion profiles for the respective parallel-helix bundles *p2'gpo5* and *p2'gph5* are shown in Fig. 8 A, B respectively. The profiles for the truncated-helix models (solid curves) are compared with those of the corresponding 23-residue helix models (dotted curves). It is clear that there is little difference between those regions of the profiles corresponding to residues 1–15. *Minor* differences are seen in the regions corresponding to the C-terminal extensions of the longer helices. Thus one may conclude that observations made within this paper are robust to the exact length of the M2 helices, provided that the 4-8-12 motif-containing region is helical.

Discussion

Implications of modelling studies

The modelling studies clearly indicate that channel-ion interactions in M2-analogue helix bundle models are strongly dependent upon the χ_1 and χ_2 values of polar sidechains at positions 4, 8, and 12. Permitted χ_1 values are primarily determined by stereochemical criteria, with the constraints being greater for T sidechains. The χ_2 values adopted are determined by electrostatic interactions between sidechain hydroxyl groups and permeant ions. It is of interest to note that neutron diffraction studies of hydroxyl hydrogen conformations in trypsin (Kossiakoff et al. 1990) revealed that, in situations where there was an incompatibility between steric and electrostatic criteria, the latter were dominant in determining Hγ positions. Furthermore, no correlations were noted between χ_1 and χ_2 values. Similar conclusions were obtained by Brünger and Karplus (1988) on the basis of empirical energy placement of polar hydrogen positions.

The "optimization" procedure introduced to determine χ_2 values for use with different permeant ions is an approximation employed in order to enable ion energy profiles to be calculated using "frozen" coordinates for channel models. An alternative is to translate the ion along z, and for each position of the ion to perform an energy minimization in which sidechain atoms are allowed to move whilst mainchain coordinates are fixed. This was used by e.g. Furois-Corbin and Pullman (1991) in their study of the nAChR. A comparable approach has been evaluated (Sansom, unpublished results) on M2 helix bundle models, and on models of channels formed by zervamicin (a peptaibol related to alamethicin; Sansom 1991; Balaram et al. 1992). Profiles thus obtained were similar to those derived via the "optimization" procedure.

Implicit in the optimization procedure is the assumption that the conformation of the sidechains, i.e. χ_2, is able to adjust as the ion moves through the channel. In the case of a permeant K^+ ion the conformational changes required are relatively small for the χ_1 $g-$ and $g+$ models, as hydrogen bonding in absence of the ion causes χ_2 to adopt values close to the "optimum". In the case of Cl^-, the requisite conformational changes are larger, as pre-existing hydrogen bonds must be broken in order to permit favourable $H\gamma-Cl$ interactions. Some support for the possibility of such a "wave" of conformational change as the ion moves through the channel arises from molecular dynamics studies of gramicidin (Mackay et al. 1984; Jordan 1990; Roux and Karplus 1991) which indicate that local deformation of mainchain carbonyl groups occurs as Na^+ ions move along the channel.

The main conclusion from the current study is that conformational flexibility at χ_2 enables both S and T residues to form favourable interactions with anions or cations. A subsidiary conclusion is that there is thus no apparent difference between S and T residues in their interactions with permeant ions, other than the inability of the latter to adopt the $\chi_1 = t$ conformation. As all three classes of model (i.e. $\chi_1 = g-$, $g+$ and t) are capable of generating favourable interactions with both anions and cations, this suggests that the presence of T vs. S residues within the 4-8-12 motif is not a principal mechanism whereby anion/cation selectivity may be generated.

The studies on 4-8-12 motif models described in this paper are related to two other investigations, both of which concern models of complete nAChR M2 helices. Furois-Corbon and Pullman (1989a, b; 1991) have studied a tilted-helix bundle model employing 21-residue *Torpedo* nAChR α, β, γ and δ M2 sequences. Negatively charged sidechains at position 1 were included in this model. Model coordinates were frozen except for the sidechains of 4, 8, 12, 15 and 19, and the probe was an Na^+ ion. The resultant energy profile showed energy minima corresponding to residues 4, 8 and 12 comparable to those seen in the current study, in addition to minima at positions 1 and 15. However, analysis of sidechain conformations was not presented, and anion probes were not explored. Eisenman and Alvarez (1991) performed an energy profile calculation on the *Torpedo* nAChR M2 δ model of Oiki et al. (1988), using the protein-dipole Langevin-dipole algorithm of Warshel and Russell (1984). Their approach resembled that employed here in that two alternative χ_2 values were explored for hydroxyl sidechains, one for a Cs^+ ion probe and one for a Cl^-. However, detailed information on sidechain conformations (in particular χ_1 values) was not reported. An important aspect of the current study is the attempt to relate conformational properties of channel-lining sidechains to their interactions with permeant ions.

Overall, the current study complements and confirms the picture of nAChR channel structure emerging from site-directed mutagenesis and related studies. The latter suggest that ion selectivity is conferred on the channel by "rings" of charged residues at either entrance to the pore – the co-called cytoplasmic, intermediate and extracellular rings. The 4-8-12 motif therefore provides a series of transient, non-selective binding sites for either anions or cations. Either S or T residues may be employed as ligands for the permeant ions.

An interesting corollary of these conclusions is the prediction that a channel lined solely with S should be permeable to both anions and/or cations. Lear et al. (1988) synthesized a 21-mer S-rich peptide $(L-S-S-L-L-S-L)_3-NH_2$, and demonstrated that it formed *cation* selective channels in planar lipid bilayers. Model-building studies suggested an $N = 6$ parallel-helix bundle for the structure of the channel. It is unclear why such a channel cannot permit, anions to pass through it, simply by switching the χ_2 values appropriately. Conceivably the network of hydrogen bonds within the lining of the channel is such as to lock the χ_2 torsions into an *"o"* conformation, thus generating cation selectivity.

Possible extensions of the models

This paper focuses on the 4-8-12 sequence motif. Clearly M2 helices of members of the nAChR superfamily are more complex with respect to their possible interactions with ions. Furthermore, ion channels interact not only with inorganic, ions but with larger, impermeable organic ions (i.e. open-channel blockers). There are two directions in which the models employed in this paper may be extended: (a) incorporation of more complex M2 sequence motifs; and (b) modelling of channel-blocker interactions.

More complex motifs. The most immediate extension to the 4-8-12 motif is to incorporate residue 15. This is a conserved T in anion selective channels and is generally a V (more rarely I or A) in cation selective channels (see Table 1). On a helical wheel projection it lies between residues 4 and 8 and thus is directed towards the centre of the pore. Incorporation of T15 would be expected to add an additional energy minimum to ion profiles.

In the current models residue 11 is located close to the helix-helix interface. Position 11 is a conserved hydrophobic residue, generally L (more rarely F). Revah et al. (1991) constructed various L11 mutants of nAChR α7. Mutant L11T had a decreased rate of desensitization and

exhibited an additional conductance level in single channel recordings. A possible explanation is that L11 normally occludes the channel when in the desensitized conformation. Incorporation of L11 in M2 bundle models may provide valuable clues as to changes in bundle geometry which occur during the sequence of conformational changes (closed ⇒ open ⇒ desensitized) which occurs following exposure of nAChR to acetylcholine.

Finally, it would be of interest to incorporate E1 into the models. This residue forms the "intermediate ring" of anionic residues, which mutagenesis studies (Konno et al. 1991) have shown to be a major determinant of nAChR ion selectivity. On a helical wheel projection E1 lies between residues 8 and 12 and thus is directed towards the lumen of the channel. Several problems might be associated with incorporation of E1 into the models: (a) it is a flexible sidechain and one might need to consider helix bundle models in which the five E1 sidechains adopt different conformations (Sansom, unpublished results); (b) the local pK_a of E1 is not known and may differ from its free solution value, given the presence of several such sidechains in relatively close proximity; and (c) at any one time, not all of the E1 sidechains in a bundle need be dissociated. If exploring the properties of *single* channels then (c) might have to be treated in a stochastic fashion.

Open-channel blockers. Open-channel blockers are large organic ions which are believed to bind to the pore of an open channel in a voltage-dependent fashion, thus occluding it and preventing passage of ions (Hille 1984). The local anaesthetic derivative QX-222 is an open-channel blocker of nAChR which has been studied in some detail. It has a bulky aromatic residue linked to a trimethylammonium group. Mutations S8A and S12A (Leonard et al. 1988; Charnet et al. 1990) decreased the affinity of nAChR for QX-222, implicating these residues in hydrogen-bond interactions with the blocker. Certain mutations of L11 of $\alpha 7$ (L11T and L11S, but not L11V and L11F) abolish block by QX-222 (Revah et al. 1991), implicating L11 in hydrophobic interactions with the blocker. Combining such information with electrophysiological data on the voltage dependence of QX-222 block should enable development of a model for QX-222 interactions with simplified M2 bundle models in order to provide a reasonably accurate representation of the interactions of the blocker with the intact receptor.

nAChR and various Glu-R (including NMDA-R) are blocked by a variety of toxins which are based upon a spermine-like polyamine group, of which the most intensively studied is philanthotoxin (PhTx; Eldefrawi et al. 1988). As for QX-222, PhTx is believed to bind within the lumen of the open channel. Preliminary modelling studies (Sansom, unpublished results) suggest that the structure of spermine is closely complementary to that of the 4-8-12 motif. Studies are currently underway to develop stuctural models of polyamine toxin interactions with M2 bundle models. These are of particular interest as quantitative structure-activity data is available for binding of a wide range of PhTx analogues to nAChR and to NMDA-R (Anis et al. 1990).

Methodological limitations

Two aspects of the methodology merit further discussion. The first is the absence of any (explicit) representation of solvent in the models. The primary reason for this is that the study was designed to provide a structural rationalization of a motif found in amino acid sequences of receptor-channel proteins, rather than to calculate true ion permeation profiles. Thus ion solvation/desolvation processes were not taken into consideration. An attempt to accommodate solvent screening of electrostatic interactions was made via use of a distance dependent dielectric. As demonstrated in an earlier paper (Sansom et al. 1991), although one may argue for and against such a model (e.g. Gilson and Honig 1988), adoption of different models for the dielectric does not qualitatively alter the resultant channel-ion interaction profiles.

The second aspect of the methodology meriting attention is the "helix dipole subtraction" procedure. In one respect, this may be viewed merely as a computational device for "uncovering" the interactions of a permeant ion with the 4-8-12 motif. More rigorously, the procedure is justified given that: (a) rings of anionic residues; and (b) an outer bundle of oppositely oriented helix dipoles, are able to compensate for the helix dipole effect in the intact nAChR and related proteins. This has been demonstrated both using models similar to those explored above (Sansom, unpublished observations), and for models or *Torpedo* nAChR (Eisenman and Alvarez 1991; Furois-Corbin and Pullman 1989b; 1991). As discussed by e.g. Richardson and Richardson (1989), glutamate residues at position 1 of α-helices tend to neutralize the helix dipole.

Several possible improvements to procedures adopted in this study may be pursued. Generation of helix bundles may be refined so as to eliminate "intuitive" selection of input parameters (θ, R, Ω). We are currently investigating the use of hydrophilic surface maps (Kerr and Sansom 1992) in order to define θ more objectively prior to construction of initial bundle models. These models may then be refined via simulated annealing methods (Chou and Carlucci 1991). Nilges and Brünger (1991) have used a simulated annealing protocol to investigate the coiled-coil structure of a leucine zipper. Preliminary investigations (Doak, Kerr and Sansom, unpublished observations) suggest that a similar procedure may be successfully employed to refine a helix bundle model of the ion channel formed by *Staphylococcus aureus* δ-toxin. It may prove necessary to incorporate a (simplified) representation of the bilayer environment into such calculations (see e.g. Wang and Pullman 1991).

Treatment of ion solvation/desolvation would enable true permeation profiles to be calculated. This has been achieved by several workers (Åqvist and Warshel 1989; Roux and Karplus 1991) applying free energy perturbation calculations to gramicidin channels. However, it would probably be desirable to improve the 4-8-12 motif models (see above) before carrying out such calculations. A possible alternative to such calculations may lie in diffusion-based simulations of ion permeation using numerical solution of the linearized Poisson-Boltzmann equa-

tion to evaluate electrostatic interactions, followed by Brownian dynamics simulations (Davis et al. 1991). This approach has been successfully employed in studies of enzyme-ligand association kinetics (e.g. Madura and McCammon 1989). Brownian dynamics simulations of ion permeation have already been carried out for rather more abstract models of ion channels (Cooper et al. 1985). Overall, one might envisage attempting to combine molecular dynamics simulations for short timescale information, with Brownian dynamics or related simulation methods for longer timescale behaviour (see discussion in Dani and Levitt 1990).

Acknowledgements. This work was supported by The Wellcome Trust. My thanks to Dr. Graham Richards for providing access to computational facilities, and to Prof. Louise Johnson for valuable advice concerning the conformational properties of threonine sidechains.

References

Anis N, Sherby S, Goodnow RA, Niwa M, Konno K, Kallimopoulos T, Bukownik R, Nakanishi K, Usherwood PNR, Eldefrawi A, Eldefrawi M (1990) Structure-activity relationships of philanthotoxin analogs and polyamines on N-methyl-D-aspartate and nicotinic acetylcholine receptors. J Pharm Exp Therap 254:764–773

Åqvist J, Warshel A (1989) Energetics of ion permeation through membrane channels: solvation of Na^+ by gramicidin A. Biophys J 56:171–182

Arnott S, Wonacott A (1966) Atomic coordinates for an α-helix: refinement of the crystal structure of α-poly-L-alanine. J Mol Biol 21:371–383

Baker EN, Hubbard RE (1984) Hydrogen bonding in globular proteins. Prog Biophys Mol Biol 44:97–179

Balaram P, Sukumar M, Krishna K, Mellor IR, Sansom MSP (1992) The properties of ion channels formed by zervamicins Eur Biophys J 21:117–128

Betz H (1990) Homology and analogy in transmembrane channel design: lessons from synaptic membrane proteins. Biochem 29:3591–3599

Brooks CL, Karplus M, Pettitt BM (1988) Proteins: a theoretical perspective of dynamics, structure, and thermodynamics. Wiley, New York

Brooks BR, Bruccoleri RE, Olafson BD, States DJ, Swaminathan S, Karplus M (1983) CHARMM: a program for macromolecular energy, minimization, and dynamics calculations. J Comp Chem 4:187–217

Brünger AT, Karplus M (1988) Polar hydrogen positions in proteins: empirical energy placement and neutron diffraction comparison. Proteins: Struct Func Genet 4:148–156

Capaldi RA (1982) Structure of intrinsic membrane proteins. Trends Biochem Sci 7:292–295

Charnet P, Labarca C, Leonard RJ, Vogelaar NJ, Czyzyk L, Gouin A, Davidson N, Lester HA (1990) An open-channel blocker interacts with adjacent turns of α-helices in the nicotinic acetylcholine receptor. Neuron 2:87–95

Chou KC, Carlucci L (1991) Simulated annealing approach to the study of protein structures. Prot Eng 4:661–667

Cooper K, Jakobson E, Wolynes P (1985) The theory of ion transport through membrane channels. Prog Biophys Mol Biol 46:51–96

Couturier S, Bertrand D, Matter JM, Hernandez MC, Bertrand S, Millar N, Valera S, Barkas T, Ballivet M (1990) A neuronal nAChR subunit α7 is developmentally regulated and forms a homooligomeric channel blocked by α-BTX. Neuron 5:847–856

Dani JA, Levitt DG (1990) Diffusion and kinetic approaches to describe permeation in ionic channels. J Theor Biol 146:289–301

Davis ME, Madura JD, Luty BA, McCammon A (1991) Electrostatics and diffusion of molecules in solution: simulations with the University of Houston Brownian dynamics program. Comp Phys Comm 62:187–197

Eisenman G, Alvarez O (1991) Structure and function of channels and channelogs as studied by computational chemistry. J Membr Biol 119:109–132

Eldefrawi AT, Eldefrawi ME, Konno K, Mansour NA, Nakanishi K, Oltz E, Usherwood PNR (1988) Structure and synthesis of a potent glutamate receptor antagonist in wasp venom. Proc Natl Acad Sci USA 85:4910–4913

Furois-Corbin S, Pullman A (1986) Theoretical study of the packing of α-helices by energy minimization: effect of the length of the helices on the packing energy and on the optimal configuration of a pair. Chem Phys Lett 123:305–310

Furois-Corbin S, Pullman A (1989a) A possible model for the inner wall of the acetylcholine receptor channel. Biochim Biophys Acta 984:399–350

Furois-Corbin S, Pullman A (1989b) Energy profiles in the acetylcholine receptor (AChR) channel. FEBS Lett 252:63–68

Furois-Corbin S, Pullman A (1991) The effect of point mutations on energy profiles in a model of the nicotinic acetylcholine receptor (AChR) channel. Biophys Chem 39:153–159

Galzi JL, Revah F, Bessis A, Changeux JP (1991) Functional architecture of the nicotinic acetylcholine receptor: from electric to brain. Ann Rev Pharmacol Toxicol 31:37–72

Gilson MK, Honig BH (1988) Energetics of charge-charge interactions in proteins. Proteins: Str Func Genetics 3:32–52

Giraudat J, Dennis, M, Heidmann T, Haumont PY, Lederer F, Changeux JP (1987) Structure of the high-affinity binding site for noncompetitive blockers of the acetylcholine receptor: [3H] chlorpromazine labels homologous residues in the β and δ chains. Biochem 26:2410–2418

Goodford PJ (1985) A computational procedure for determining energetically favorable binding sites on biologically important macromolecules. J Med Chem 28:849–857

Gray TM, Matthews BM (1984) Intrahelical hydrogen bonding of serine, threonine and cysteine residues within α-helices and its relevance to membrane-bound proteins. J Mol Biol 175:75–81

Grenningloh G, Rienitz A, Schmitt B, Methfessel C, Zensen M, Beyreuther K, Gundelfinger ED, Betz H (1987) The strychnine-binding subunit of the glycine receptor shows homology with nicotinic acetylcholine receptors. Nature 328:215–220

Hille B (1984) Ionic Channels of Excitable Membranes. Sinauer Associates Inc., Sunderland, Mass

Hol WG, von Duijen PT, Berendsen HJC (1978) The α-helix dipole and the properties of proteins. Nature 273:443–446

Hollman M, O'Shea-Greenfield A, Rogers SW, Heinemann S (1989) Cloning by functional expression of a member of the glutamate-receptor family. Nature 342:643–648

Hucho F, Oberthür W, Lottspeich F (1986) The ion channel of the nicotinic acetylcholine receptor is formed by the homologous helices M II of the receptor subunits. FEBS Lett 205:137–142

Imoto K, Busch C, Sakmann B, Mishina M, Konno T, Nakai J, Bujo H, Mori Y, Fukuda K, Numa S (1988) Rings of negatively charged amino acids determine the acetylcholine receptor channel conductance. Nature 335:645–648

Imoto K, Konno T, Nakai J, Wang F, Mishina M, Numa S (1991) A ring of uncharged polar amino acids as a component of channel constriction in the nicotinic acetylcholine receptor. FEBS Lett 289:193–200

Jordan PC (1990) Ion-water and ion-polypeptide correlations in a gramicidin-like channel: molecular dynamics study. Biophys J 58:1133–1156

Keinanen K, Wisden W, Sommer B, Werner P, Herb A, Verdoorn TA, Sakmann B, Seeburg PH (1990) A family of AMPA-selective glutamate receptors. Science 249:556–560

Kerr ID, Sansom MSP (1992) Hydrophilic surface maps of channel-forming peptides. Biochem Soc Trans 20:323S

Konno T, Busch C, von Kitzing E, Imoto K, Wang F, Nakai J, Mishina M, Numa S, Sakmann B (1991) Rings of anionic amino acids as structural determinants of ion selectivity in the acetylcholine receptor channel. Proc Roy Soc B 244:69–79

Kossiakoff AA, Shpungin J, Sintchak MD (1990) Hydroxyl hydrogen conformations in trypsin determined by the neutron diffraction solvent difference map method: relative importance of steric and electrostatic factors in defining hydrogen-bonding geometries. Proc Natl Acad Sci USA 87:4468–4472

Kraulis PJ (1991) MOLSCRIPT: a program to produce both detailed and schematic plots of protein structures. J Appl Cryst 24:946–950

Lear JD, Wasserman ZR, DeGrado WF (1988) Synthetic amphiphilic peptide models for protein ion channels. Science 240:1177–1181

Leonard RJ, Labarca CG, Charnet P, Davidson N, Lester HA (1988) Evidence that the M2 membrane-spanning region lines the ion channel pore of the nicotinic receptor. Science 242:1578–1581

Mackay DHJ, Berens PH, Wilson KR, Hagler AT (1984) Structure and dynamics of ion transport through gramicidin A. Biophys J 46:229–248

Madura JD, McCammon JA (1989) Brownian dynamics simulation of diffusional encounters between triose phosphate isomerase and D-glyceraldehyde phosphate. J Phys Chem 93:7285–7287

Maricq AV, Peterson AS, Brake AJ, Myers RM, Julius D (1991) Primary structure and functional expression of the 5 HT_3 receptor, a serotonin-gated ion channel. Science 254:432–436

Mitra AK, McCarthy MP, Stroud RM (1989) Three-dimensional structure of the nicotinic acetylcholine receptor and location of the major associated 43-kD cytoskeletal protein, determined at 22 Å by low dose electron microscopy and X-ray diffraction to 12.5 Å. J Cell Biol 19:755–774

Moriyoshi K, Masu M, Ishii T, Shigemoto R, Mizuno N, Nakanishi S (1991) Molecular cloning and characterization of the rat NMDA receptor. Nature 354:31–37

Nilges M, Brünger AT (1991) Automated modeling of coiled coils: application to the GCN4 dimerization region. Prot Eng 4:649–659

Noda M, Takahashi H, Tanabe T, Toyosato M, Kikyotani S, Furutani Y, Hirose T, Takashima H, Inayama S, Miyata T, Numa S (1983) Structural homology of *Torpedo californa* acetylcholine receptor subunits. Nature 302:528–532

Oiki S, Danho W, Madison V, Montal M (1988) M2δ, a candidate for the structure lining the ionic channel of the nicotinic acetylcholine receptor. Proc Natl Acad Sci USA 85:8703–8707

Pritchett DB, Sontheimer H, Shivers B, Ymer S, Kettenmann H, Schofield PR, Seeburg PH (1989) Importance of a novel $GABA_A$ receptor subunit for benzodiazepine pharmacology. Nature 338:582–584

Revah F, Bertrand D, Galzi JL, Devillers-Thiery A, Mulle C, Hussy N, Bertrand S, Ballivet M, Changeux JP (1991) Mutations in the channel domain alter desensitization a neuronal nicotinic receptor. Nature 353:846–849

Richardson JS, Richardson DC (1989) Principles and patterns of protein conformation. In: Fasman GD (ed) Prediction of Protein Structure and the Principles of Protein Conformation. Plenum Press, New York, pp 1–98

Rogers NK (1986) The modelling of electrostatic interactions in globular proteins. Prog Biophys Mol Biol 48:37–66

Roux B, Karplus M (1991) Ion transport in a model gramicidin channel: structure and thermodynamics. Biophys J 59:961–981

Sansom MSP (1991) The biophysics of peptide models of ion channels. Prog Biophys Mol Biol 55:139–235

Sansom MSP, Kerr ID, Mellor IR (1991) Ion channels formed by amphipathic helical peptides – a molecular modelling study. Eur Biophys J 20:229–240

Sansom MSP (1992) Proline residues in transmembrane helices of channel and transport proteins: a molecular modelling study. Prot Eng 5:53–60

Schofield PR, Darlison MG, Fujita N, Bart DR, Stephenson FA, Rodriguez H, Rhee LM, Ramachadran J, Reale V, Glencorse TA, Seeburg PH and Barnard EA (1987) Sequence and functional expression of the $GABA_A$ receptor shows a ligand-gated receptor superfamily. Nature 328:221–227

Stroud RM, McCarthy MP, Shuster M (1990) Nicotinic acetylcholine receptor superfamily of ligand gated ion channels. Biochem 29:11007–11023

Toyoshima C, Unwin N (1990) Three-dimensional structure of the acetylcholine receptor by cryoelectron microscopy and helical image reconstruction. J Cell Biol 111:2623–2635

Toyoshima C, Unwin N (1988) Ion channel of acetylcholine receptor reconstructed from images of postsynaptic membranes. Nature 336:247–250

Unwin N (1989) The structure of ion channels in membranes of excitable cells. Neuron 3:665–676

Villarroel A, Herlitze S, Koenen M, Sakman B (1991) Location of a threonine residue in the α-subunit M2 transmembrane segment that determines the ion flow through the acetylcholine receptor channel. Proc R Soc Lond B 243:69–74

Wang J, Pullman A (1991) Do helices in membranes prefer to form bundles or to stay dispersed in the lipid phase? Biochim Biophys Acta 1070:493–496

Warshel A, Russell ST (1984) Calculation of electrostatic interactions in biological systems and in solutions. Q Rev Biophys 17:283–422